厚生労働科学研究費補助金

創薬基盤推進研究事業

ヒト肝細胞キメララットによる新しい創薬評価モデルの開発

平成23年度～平成24年度　総合研究報告書

研究代表者　真下　知士

平成２５（２０１３）年　６月

目　　次

厚生労働科学研究費補助金（創薬基盤推進研究事業）
（総合）研究報告書

ヒト肝細胞キメララットによる新しい創薬評価モデルの開発に関する研究

研究代表者　　真下　知士　　特定准教授

研究要旨
本研究では、ジンクフィンガーヌクレアーゼ（ZFN）技術により重症免疫不全SCIDラットを作製し、ヒト肝細胞を移植することで、ラット体内にヒト肝臓代謝システムを構築する。開発された肝ヒト化ラットは、新規医薬品のスクリーニング、薬理薬効試験、薬物動態試験、毒性試験等を効果的に実現することができる新たな創薬モデル基盤の開発に繋がる。

研究分担者
なし

A. 研究目的

創薬候補化合物のスクリーニングおよび前臨床試験では必ず動物実験が行われるが、ヒト薬物動態を正確に予測するためには、動物ーヒト種間での肝臓代謝酵素の違いが問題になることが多い。本研究では、新しい遺伝子改変技術ジンクフィンガーヌクレアーゼ（ZFN）により作製した重症免疫不全ラットに、ヒト肝細胞を移植して模擬的なヒト肝臓を構築することにより、ラット体内でヒト薬物代謝試験を行える新たな創薬モデル基盤を開発する。

B. 研究方法

平成23年度に、ZFN 技術によりSCID 、XSCID、およびダブルSCID（FSG）ラットを作製した。これら重症免疫不全ラットにおいて、血中グロブリンレベル、T細胞、B細胞、NK細胞などをFACS解析した。さらに、これら免疫不全ラットの免疫応答を評価するため、ヒト卵巣がん細胞を皮下移植、ヒトiPS細胞の精巣移植を実施した。

平成24年度は、これら重症免疫不全ラットに、ヒト肝細胞を移植することで高効率にヒト肝細胞が置換されたキメララットを作製した。作製したキメララットにおいて、ヒトアルブミン生産能、ヒト薬物代謝酵素機能、ヒト肝細胞置換率を測定した。

C. 研究結果

平成23年度は、ZFN 技術によりSCID 、XSCID、およびダブルSCID（FSG）ラットを作製した。FSGラットにおいて、血中グロブリンレベルの欠失、T細胞、B細胞、NK細胞の欠失など重度の免疫機能不全を確認した。このFSGラットを用いて、1）ヒト卵巣がん細胞を皮下で増殖させること、2）ヒトiPS細胞を精巣に移植することでテラトーマの形成に成功した。

平成24年度は、この重症免疫不全ラットにヒト肝細胞を移植することで、肝ヒト化ラットの作製を試みた。ラット肝細胞の増殖を阻害するアルカロイドの一種であるレトロルシンを投与した後、FSGラットの門脈からヒト肝細胞を移植した。ヒト肝細胞移植後からすぐに、ヒトアルブミンがラット血中に持続的に検出された。移植6週後にはFSGラットの肝臓内に、ヒト肝細胞の生着および増殖が確認された。さらに、ヒト間葉系幹細胞から分化したヒト肝細胞様細胞を移植したFSGラットの血中において、ヒトアルブミンを検出することに成功した。

D. 考察

本研究において、ZFN技術により作製した重症免疫不全ラットに、ヒト肝細胞を移植して模擬的なヒト肝臓を構築することに成功した。今後は、ラット肝臓内におけるヒト肝細胞の置換率の向上を目指す。ラットは、マウスよりも体が10倍大きく、肝細胞、血液、胆汁採取等にメリットがある。高効率の肝ヒト化ラットを利用することで、創薬候補化合物のスクリーニング、新規医薬品の薬物代謝、薬効・毒性試験、薬物間相互作用をヒト生体レベルで評価することが可能となる。

E. 結論

本研究により、重症免疫不全ラットを開発し、ヒト肝細胞を移植した肝ヒト化ラットの作製に成功した。重症免疫不全SCID 、XSCID、およびFSGラットは、ナショナルバイオリソースプロジェクト「ラット」を通して国内外研究機関へ提供するとともに、ヒト肝細胞キメララットについてはフェニックスバイオからの販売を検討する。

F. 健康危険情報

なし

G. 研究発表

1．論文発表

*Mashimo T, Kaneko T, Sakuma T, Kobayashi J, Kunihiro Y, Voigt B, Yamamoto T, Serikawa T. Efficient gene targeting by TAL effector nucleases coinjected with exonucleases in zygotes. ***Scientific Reports*** 3: 1253, 2013

*Mashimo T, Takizawa A, Kobayashi J, Kunihiro Y, Yoshimi K, Ishida S, Tanabe K, Yanagi A, Tachibana A, Hirose J, Yomoda J, Morimoto S, Kuramoto T, Voigt B, Watanabe T, Hiai H, Tateno C, Komatsu K, Serikawa T. Generation and Characterization of Severe Combined Immune Deficient Rats. ***Cell Reports*** 2(3):685-94, 2012

Ishida S, Sakamoto Y, Nishio T, Baulac S, Kuwamura M, Ohno Y, Takizawa A, Kaneko S, Serikawa T, *Mashimo T: Kcna1-mutant rats dominantly display myokymia, neuromyotonia and spontaneous epileptic seizures. ***Brain Research*** 1435: 154-66, 2012

*Baulac S, Ishida S, *Mashimo T, Boillot M, Fumoto N, Kuwa mura M, Ohno Y, Takizawa A, Aoto T, Ueda M, Ikeda A, Leguern E, Takahashi R, Serikawa T. A rat model for Lgi1-related epilepsies. ***Hum Mol Genet.*** 21(16): 3546-57, 2012

Asahina M, Mashimo T, Takeyama M, Tozawa R, Hashimoto T, Takizawa A, Ueda M, Aoto T, Kuramoto T, Serikawa T. Hypercholesterolemia and atherosclerosis in low density lipoprotein receptor mutant rats. ***Biochem Biophys Res Commun.*** 418(3): 553-8, 2012

2．学会発表

真下 知士「遺伝子改変ラットの開発研究」第 6 回ラットリソースリサーチ研究会・第 1 回実験動物科学シンポジウム、京都、2013 年 2 月 1 日

真下 知士、芹川忠夫「ラットを中心とした遺伝子改変動物研究の現状」第 85 回日本生化学会大会、福岡、福岡国際会議場、2012 年 12 月 16 日

真下 知士、小林 純也、小松 賢志、芹川忠夫「DNA-PK のラット特異的な機能制御について」第 35 回日本分子生物学会、福岡、福岡国際会議場、2012 年 12 月 13 日

芹川忠夫、金子武人、佐久間哲史、山本 卓、真下知士「ラットにおける遺伝子改変技術の新展開」第 35 回日本分子生物学会、福岡、福岡国際会議場、2012 年 12 月 12 日

Mashimo T, Kaneko T, Sakuma T, Kobayashi J, Kunihiro Y, Voigt B, Yamamoto T, Serikawa T. Efficient gene targeting by TAL effector nucleases in rats. Rat Genomics and Models 2012, Cambridge, UK, Dec 3-6, 2012

Mashimo T, Kaneko T, Sakuma T, Kobayashi J, Kunihiro Y, Voigt B, Yamamoto T, Serikawa T. Efficient gene targeting by TAL effector nucleases coinjected with exonucleases in zygotes. Techniques and Procedures for Rat Gene Targeting, Reproduction, and Cryopreservation, Cambridge, UK, Dec 3, 2012

Mashimo T, Takizawa A, Kobayashi J, Komatsu K, Serikawa T. Generation of severe combined immune deficient (SCID) rats. The 4th EMBO Meeting, Nice France Sep22-25, 2012

真下知士、金子武人、国広弥生、芹川忠夫「TALEN を用いた遺伝子改変ラットの効率的な作製方法」第 2 回ゲノム編集研究会、岡崎、岡崎コンファレンスセンター、2012 年 9 月 20 日

真下知士・芹川忠夫「新たに作製した免疫不全症モデルの創薬への応用（ZFN・TALEN 遺伝子改変技術/SCID ラット）」ＤＳＡＮＪ疾患別商談会（免疫、炎症、アレルギー性疾患領域）、大阪、大阪産業創造館、2012 年 8 月 29 日

真下知士「TALEN 技術について」平成 24 年度和光純薬工業代理店夏期講習会、大阪、和光純薬工業株式会社、2012 年 8 月 21 日

真下　知士、金子　武人、国広　弥生、佐久間哲史、山本　卓、芹川　忠夫「人工ヌクレアーゼ TALEN によるノックアウトラットの作製」第 59 回日本実験動物科学・技術　九州 2012、別府国際コンベンションセンター、2012 年 5 月 25 日

真下知士「SCID rats as an animal model for preclinical xenotransplantation」京都大学医学研究科大学院教育コース腫瘍学エリアミーティング、京都、2012 年 5 月 17 日

真下知士「重症免疫不全 SCID ラットとその応用研究について」第 5 回ラットリソースリサーチ研究会、京都、2012 年 2 月 3 日

Mashimo T: Zinc-finger nucleases (ZFNs) as gene-targeting technology in animals. 第 34 回日本分子生物学会、横浜、2011 年 12 月 13 日

真下知士、芹川忠夫「ラット遺伝子改変技術のめざましい進歩」第 47 回高血圧関連疾患モデル学会学術総会、札幌、2011 年 9 月 6 日

真下知士「遺伝子改変動物作製技術の新しい展

開」シグマアルドリッチ ライフサイエンスセミナー 2011、大阪、2011 年 8 月 25 日

真下知士「ZFN による遺伝子改変ラットの作製法」自然科学研究機構・基礎生物学研究所共同利用共同研究・研究会、岡崎、2011 年 7 月 11 日

真下知士「ジンクフィンガーヌクレアーゼを利用した遺伝子改変動物の作製」第 58 回日本実験動物学会総会、東京、2011 年 5 月 27 日

Mashimo T: Zinc-finger nucleases (ZFNs) as gene-targeting technology in animals. University of Queensland, Brisbane, Australia, May 11, 2011

Mashimo T: Zinc-finger nucleases (ZFNs) as gene-targeting technology in animals. Queensland Institute of Medical Research, Brisbane, Australia, May 10, 2011

Mashimo T: Zinc-finger nucleases (ZFNs) as gene-targeting technology in animals. University of Technology Sydney, Sydney, Australia, May 9, 2011

Mashimo T: Creation of Knockout Rats Using Zinc-Finger Nucleases. Australasian Gene Therapy Society Meeting, Melbourne, Australia, May 4, 2011

Mashimo T: Zinc-finger nucleases (ZFNs) as gene-targeting technology in animals. Auckland University Medical School, Auckland, New Zealand, May 3, 2011

真下知士「ラット遺伝子改変技術の進歩：ヒト化ラットの開発に向けて」AK 拠点招聘セミナー、京都、2011 年 4 月 20 日

H. 知的財産の出願・登録状況

1．特許取得

なし

2．実用新案登録

なし

3．その他

なし

書籍

著者氏名	論文タイトル名	書籍全体の編集者名	書　籍　名	出版社名	出版地	出版年	ページ
真下知士	ジンクフィンガーヌクレアーゼ（ZFN）による重症免疫不全（SCID）ラットの作製と創薬応用研究への試み	戸口田淳也、池谷真	遺伝子医学MOOK 22号	株式会社メディカルドゥ	大阪	2012	44-51

雑誌

発表者氏名	論文タイトル名	発表誌名	巻号	ページ	出版年
真下知士、金子武人	ラットにおける遺伝子改変技術の新展開	細胞工学	32(5)	564-568	2013
真下知士	新たなゲノム編集技術「CRISPR/Cas」	実験医学	31(6)	892-893	2013
真下知士、芹川忠夫	ジンクフィンガーヌクレアーゼ（ZFN）	細胞工学	31(3)	296-301	2012
真下知士、芹川忠夫	ジンクフィンガーヌクレアーゼによる遺伝子改変動物の作製	MSD(メディカル・サイエンス・ダイジェスト)	38(1)	10-11	2012

SCIENTIFIC REPORTS

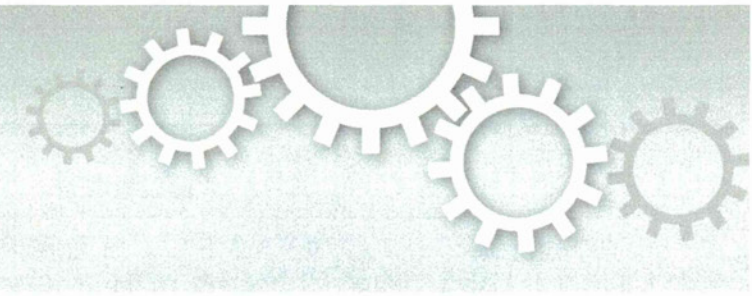

OPEN

SUBJECT AREAS:
GENE TARGETING
TRANSGENIC ORGANISMS
GENETIC ENGINEERING
MUTAGENESIS

Received
31 October 2012

Accepted
4 January 2013

Published
13 February 2013

Correspondence and requests for materials should be addressed to T.M. (tmashimo@anim.med.kyoto-u.ac.jp)

Efficient gene targeting by TAL effector nucleases coinjected with exonucleases in zygotes

Tomoji Mashimo[1], Takehito Kaneko[1], Tetsushi Sakuma[2], Junya Kobayashi[3], Yayoi Kunihiro[1], Birger Voigt[1], Takashi Yamamoto[2] & Tadao Serikawa[1]

[1]Institute of Laboratory Animals, Graduate School of Medicine, Kyoto University, Kyoto 606-8501, Japan, [2]Department of Mathematical and Life Sciences, Graduate School of Science, Hiroshima University, Higashi-Hiroshima 739-8526, Japan, [3]Genome Repair Dynamics, Radiation Biology Center, Kyoto University, Kyoto 606-8501, Japan.

TAL Effector Nucleases (TALENs) are versatile tools for targeted gene editing in various species. However, their efficiency is still insufficient, especially in mammalian embryos. Here, we showed that combined expression of Exonuclease 1 (*Exo1*) with engineered site-specific TALENs provided highly efficient disruption of the endogenous gene in rat fibroblast cells. A similar increased efficiency of up to ~30% with *Exo1* was also observed in fertilized rat eggs, and in the production of knockout rats for the albino (*Tyr*) gene. These findings demonstrate TALENs with *Exo1* is an easy and efficient method of generating gene knockouts using zygotes, which increases the range of gene targeting technologies available to various species.

Genetically engineered animals provide a powerful tool for the functional annotation of genes and for modeling human genetic diseases. Advances over the past 20 years in mouse embryonic stem cells and homologous recombination (HR)-mediated targeting have made this species the first choice for modeling human diseases. However, these technologies were only available in mice, and not in other species. Recently, new technologies have been developed and tested for gene disruption, and HR could prove an invaluable tool for the rapid generation of genetically modified animals. These new approaches include zinc-finger nucleases (ZFNs), comprising the DNA-binding domain of zinc-finger proteins fused with the non-specific DNA endonuclease *Fok*I[1–4], and transcription activator-like effector nucleases (TALENs), comprising an engineered array of TAL effector repeats fused to the *Fok*I nuclease domain[5–8]. These engineered nucleases can recognize long stretches of DNA sequences and introduce DNA double-strand breaks (DSBs). DSBs are mainly restored via non-homologous end-joining (NHEJ), a process that introduces small insertions or deletions (indels) at the repair junction, thereby generating mutations at the targeted sequences[1–8]. They are especially useful in previously non-permissive model organisms, such as sea urchins[9], crickets[10], medaka fish[11], or rats[12–14].

ZFNs/TALENs provide a straightforward strategy for targeted gene disruption in zygotes, resulting in rapid and cost-effective knockouts. Although both commercial and open resources are available for the design of ZFN/TALEN reagents, ZFNs present hurdles in terms of cost and protocols, making it difficult to establish ZFNs as a routine laboratory process. The sequences recognized by ZF domains are also limited, whereas TAL effectors can recognize almost any sequence, except T at position 0[5,7,8]. Simple and straightforward design and assembly strategies have been developed for rapid construction of TALENs, providing a cost-effective targeted nuclease platform. Although TALEN technologies have advantages, the technology remains uncertain because its introduction is so recent[6]. Since the original discovery of TAL effectors in the plant pathogenic bacteria, *Xanthomonas*, the system appears to be less effective in rodent embryos, such as mice and rats (unpublished data, personal communication). The larger size of the proteins may also impede the gene targeting efficiency compared with ZFNs, even though the recently reported truncation of the N- and C-terminal regions of the native proteins has increased the TALEN DSB-activity[15]. Improved methodology is needed to further exploit the utility of this technology. For example, a recent report showed that coupling designer endonucleases with DNA end-processing enzymes could improve gene disruption rates in mouse and human cells[16]. To address this issue, we co-expressed Exonuclease 1 (*Exo1*) with engineered TALENs to enhance gene targeting efficiency in rat zygotes.

Results

Construction of TAL effecter nucleases and the single-strand annealing (SSA) assay. Over 100 strains of albino rats deposited into the National Bio Resource Project – Rat (http://www.anim.med.kyoto-u.ac.jp/nbr/) have the same missense mutation (Arg299His) in the Tyrosinase (*Tyr*) gene[17]. The coat-color phenotype is easily and observably distinguishable for TALEN-induced mutations; therefore, we targeted the rat *Tyr* gene. A pair of TALENs was constructed using a two-step assembly method[18] with a Golden Gate TALEN kit, originally established from the Voytas lab[19] (Figure 1A). For the subsequent use of TALENs in the SSA assay, transfection into cultured cells, and mRNA synthesis, the backbone vectors for the second-step assembly were replaced with the mammalian expression vector pcDNA-TAL vector, which has CMV and T7 promoters[18]. The TALEN-based constructs were also replaced with deletion frameworks of +153 N- and +47 C-terminal domains, termed the NC scaffold, as previously reported[15] (Figure 1B).

We then performed a validation test of the mammalian cell-based SSA assay in human embryonic kidney 293T (HEK293T) cells for designed Tyr-TALENs and Tyr-TALENs-NC (Figure 1C).

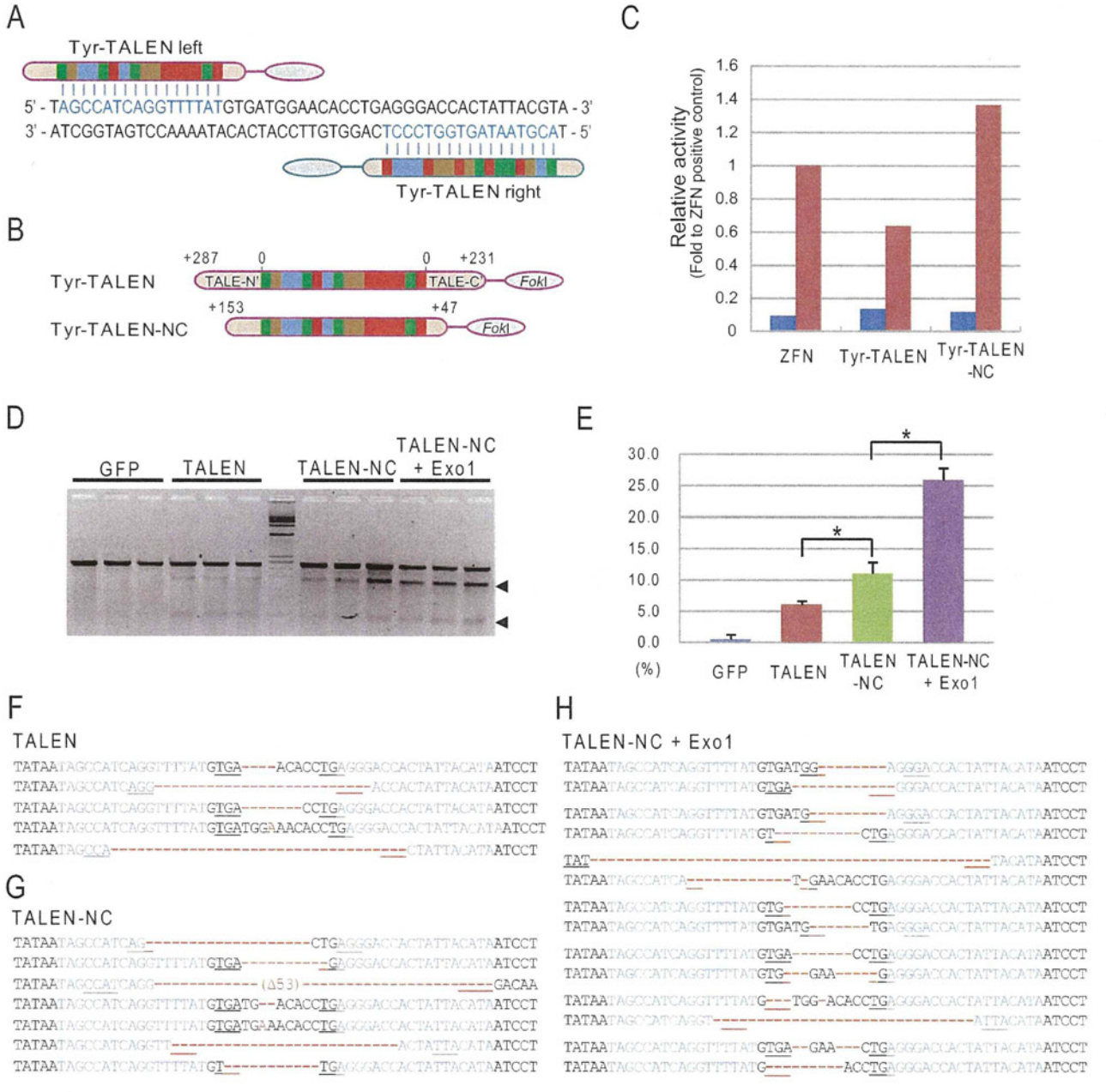

Figure 1 | TALEN constructs and the validation of their activity in rat fibroblasts. (A) Structure of engineered TALENs binding to exon 2 of rat Tyrosinase (*Tyr*) gene. (B) TALEN scaffolds (upper) and N- and C-terminal truncated scaffolds (lower), respectively. (C) Relative TALEN activity measured by a single-strand annealing (SSA) assay in human embryonic kidney 293T (HEK293T) cells. (D) Surveyor (Cel-I) nuclease assay for TALEN-induced mutations in *Tyr*. Arrowheads indicate the expected positions of the digested products. (E) Surveyor assay showing that increased frequency of TALEN-induced mutations by NC truncation and co-expression of *Exo1*. Data are expressed as means ± SEM (n = 3). *P<0.01 by Student's t-tests. (F–H) Sequence analyses showing increased mutation efficiency by NC truncation and *Exo1* expression. Microhomologous sequences adjacent to the breakpoint are underlined for TALEN (F), TALEN-NC (G), and TALEN-NC + *Exo1* (H).

Compared with the positive control (ZFN transfected cells[9]) and negative controls (reporter vectors with unrelated sequences), the cells transfected with Tyr-TALENs showed marked activation of the *luciferase* gene at about 60% of the value of the ZFN positive control. The cells transfected with Tyr-TALENs-NC showed 40% higher activity than the ZFN treated cells, indicating that the custom-engineered TALENs have the cleavage activity and that the NC truncation of TALENs increases the cleavage efficiency in the SSA assay (Figure 1C).

Combination of exonucleases with TALENs increased the efficiency of targeted gene disruption in rat fibroblasts. To assess the activity of the TALEN architectures against an endogenous gene, we electroporated Tyr-TALEN or Tyr-TALEN-NC expression vectors, and the GFP expression vector as a negative control, into Rat-1 fibroblast cells (Table 1). After 24 h, the control cells showed more than 90% GFP-positive cells, indicating sufficient transformation rates. After 72 h, cell numbers were counted, and genomic DNA was extracted and screened for TALEN-induced mutations using the Surveyor (Cel-I) nuclease assay (Figure 1D). Similar to the results of the SSA assay, TALENs-NC showed higher activity than TALENs (11.0% *vs.* 6.1%) in Rat-1 cells (Figure 1E). However, compared with our previous results using ZFNs (mutation rates ~25%[13,20]), the TALEN activity was significantly lower.

To increase the frequency of TALEN-induced mutations, we added vectors expressing the *Exo1* gene. Co-transfection of the *Exo1* vectors and TALEN-NC showed significantly higher activity (25.9%) compared with TALEN-NC alone in the Surveyor assay (Figure 1D, E). Sequence analyses of the *Tyr* loci revealed similar mutation rates to the results of the Surveyor assay: 5.7%, 7.3%, and 17.7% in TALEN, TALEN-NC, and TALEN-NC + *Exo1* transfected cells, respectively (Table 1). There was no difference in the types of indel mutation or their sizes, which ranged from a 1-bp insertion to a 53-bp deletion centered over the TALEN recognition sites (Figure 1F–H).

***Exo1* increases the frequency of TALEN-induced gene disruption in rat zygotes.** To evaluate the gene targeting efficiency of TALENs in zygotes, we microinjected mRNA of the assembled Tyr-TALEN-NC with and without *in vitro* transcribed *Exo1* mRNA into fertilized rat eggs (Figure 2A, B). After 24 h, 30–40% of the TALENs-injected embryos differentiated normally into two-cell embryos with or without *Exo1*. PCR and sequence analyses on the two-cell embryos detected a mutation rate of 5.6% (1/18) in TALEN-NC and 28.6% (4/14) in TALEN-NC with *Exo1*, indicating that *Exo1* increases the frequency of TALEN-induced mutations in zygotes (Figure 2A). Interestingly, PCR and sequence analyses revealed that TALEN-injection into fertilized eggs could introduce homozygous mutations, which could not be detected by the Surveyor assay (Figure 2C, D). This means TALEN-induced mutations created by NHEJ could be induced at the one-cell stage, presumably during the S-phase (the DNA synthesis phase) of the cell cycle, in fertilized eggs.

Coinjection of TALENs mRNA with *Exo1* mRNA into embryos provides efficient generation of knockout rats. To generate knockout rats for the albino locus by TALENs, we again microinjected mRNA for TALENs or TALENs-NC into fertilized eggs of agouti DA rats. Of 328 TALEN-injected eggs, 126 two-cell embryos (38.4%) were transferred into the oviducts of pseudopregnant Wistar female rats, and 29 (23.0%) of these embryos were successfully carried to term (Figure 3A). However, no mutant pup was detected by sequence analyses of the targeted *Tyr* locus. Microinjection of TALENs commercially obtained from Cellectis (Paris, France) delivered two mutant pups among 30 born (6.7%) (Figure 3A). When we coinjected *Exo1* mRNA with TALENs-NC, 29 two-cell embryos were obtained from 68 injected eggs (42.6%) without obvious toxicity, and of 12 pups delivered (41.4%), three founders possessed mutations comprising 5- to 29-bp deletions (25.0%) (Figure 3B, C).

One male founder showed the albino coat-color phenotype over its entire body (Figure 3B), and sequence analyses revealed that this founder carried a homozygous mutation (a 29-bp deletion) at the *Tyr* locus (Figure 3C). When we crossed the founders with the DA strains, the TALEN-induced mutations were faithfully transmitted to the next generation. For example, a male G0 founder showing a mosaic coat-color phenotype was crossed with a DA female to obtain G1 heterozygotes. Subsequent intercrossing between G1 heterozygous males and females produced homozygous albino G2 offspring (Supplementary Fig. S1).

Discussion

As far as we know, this is the first report to show that coinjection of exonuclease *Exo1* with engineered nucleases, such as TALENs, could enhance the frequency of targeted gene disruption in zygotes, and could improve the targeting efficiency to generate knockout animals. This approach provides an easy, rapid and efficient method of generating knockout animals (Supplementary Fig. S2). For example, the custom design and assembly of TALENs and their validation by the SSA assay took 1–2 weeks. Direct injection of the engineered TALENs with pre-transcribed *Exo1* into embryos, transplantation into pseudopregnant foster mothers, and identification of TALEN-induced mutants took 1 month. A homozygous mutation producing an albino G0 founder was observed 3 weeks after birth. It will be interesting to determine how TALENs targeted both alleles to produce the homozygous mutation in zygotes, as has been observed in our previous experiments with ZFNs[13]. In addition, in our *in vitro* and *in embryo* experiments, no overt toxicity was observed when overexpressing *Exo1* in conjunction with TALENs. We also observed no effect of *Exo1* on the cell cycle and cell growth, or on embryo survival and embryo development. Although *Exo1* could increase the number of mutations at off-target sites, TALENs seem to have fewer off-target effects than ZFNs[21]. Although off-target effects might play a role in cell-based experiments, in animals such unknown mutations will be "washed out" by repetitive subsequent backcrossing with the parental strain.

It remains unclear how exonucleases enhance the efficiency of TALEN-induced gene disruption in zygotes. *Exo1* is a 5′–3′ exonuclease that has a major role in DSB-repair by 5′-strand resection of DSB-ends[22–26]. There are two major pathways for DSB-repair: NHEJ and HR. Recently, a third pathway, alternative NHEJ (altNHEJ), or microhomology mediated end-joining (MMEJ), was shown to repair DSBs in the absence or failure of the classical NHEJ (cNHEJ)

Table 1 | Surveyor assay and sequencing for TALEN-induced mutations in Rat-1 fibroblasts

			Sequence analysis		
Plasmid(s)	Cell No. (1×10^5)	Surveyor assay (%)	Mutations/Colonies	Mutation Rate (%)	Average del size (bp)
GFP	2.44 ± 0.58	0.44 ± 0.71	–	–	–
TALEN	2.81 ± 0.23	6.06 ± 0.56	5/96	5.2	14.2 ± 6.5
TALEN-NC	2.72 ± 0.33	11.04 ± 1.77	7/96	7.3	17.4 ± 6.8
TALEN-NC + Exo1	3.02 ± 0.35	25.86 ± 1.91	17/96	17.7	11.9 ± 2.6

A

Injected mRNA	Injected embryos	Two-cell embryos (%)	PCR-amplified (%)	Mutations (%)
TALEN-NC	70	21 (30.0)	18 (85.8)	1 (5.6)
TALEN–NC + Exo1	59	21 (35.6)	14 (66.7)	4 (28.6)

B

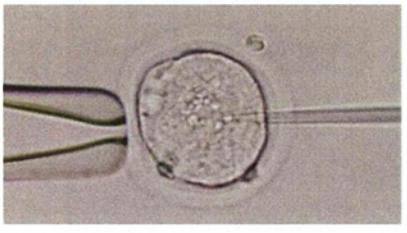

C

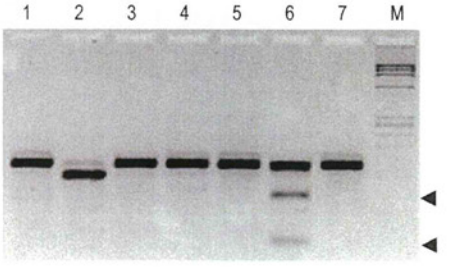

D

```
eT-NC-#8
  TATAATAGCCATCAGGTTTT------TGGAAC---TGAGGGACCACTATTACGTAATCCT
eT-NC-Exo1-#2
  TATAATAGCCATC---------(Δ24bp)---------AGGGACCACTATTACGTAATCCT
eT-NC-Exo1-#6
  TATAATAGCCATCAGGTTTTATGTGATGGAACACCTGAGGGACCACTATTACGTAATCCT
  TATAATAGCCATCAGGTTTTATGTG---------CTGAGGGACCACTATTACGTAATCCT
eT-NC-Exo1-#10
  TATAATAGCCATCAGGTTTTATGTGATGGAACACCTGAGGGACCACTATTACGTAATCCT
  TATAATAGCCATCAGGTTTTATG------GAACACCTGAGGGACCACTATTACGTAATCCT
eT-NC-Exo1-#14
  TATAATAGCCATCAGGTTTTATGTGATGGAACACCTGAGGGACCACTATTACGTAATCCT
  TATAATAGCCATCAGGTT---------(Δ29bp)----------ATTACGTAATCCT
```

Figure 2 | Targeted gene disruption by engineered TALENs in rat embryos. (A) Injection of TALEN-NC with or without *Exo1*mRNA into rat fertilized eggs. *Exo1* increased the efficiency of TALEN-induced mutations in zygotes by ~5×. (B) Microinjection of TALENs mRNA into male pronuclei of a fertilized egg. (C) Surveyor assay on the PCR products shows a TALEN-induced mutation as the digested products (arrowheads) in lane 6, but could not detect a homozygous mutation in lane 2. (D) Sequence analyses of the PCR products showed a 24-bp deletion in the homozygous alleles (eT-NC-*Exo1*-#2). Microhomologous sequences adjacent to the breakpoint are underlined.

pathway[27–29] (Figure 4). DSBs created by ZFNs or TALENs are generally repaired by cNHEJ with precise DNA-ends joining. When precise repair fails, or after the recession of DNA-ends by DNA exonucleases, DSBs would be repaired by altNHEJ, typically using closer microhomology sequences at both ends, thereby driving mutagenic end processing. Overexpression of *Exo1* probably increases DNA-end resections at the DSB-ends created by TALENs, thereby increasing the frequency of mutagenic DSB-repair via altNHEJ. To examine the effects of overexpression of *Exo1* on the NHEJ and HR pathways, we performed an NHEJ assay that measures the repair of I-SceI-generated DSBs via the NHEJ pathway[20,30] and an HR assay that measures the repair of I-SceI-generated DSBs via the HR pathway[20,31] (Supplementary Fig. S3). Those assays revealed that the *Exo1* significantly inhibited both the NHEJ pathway and the HR pathway in a wide variety of human cells (U2OS, HeLa, and MRC5), suggesting that the altNHEJ pathway would be enhanced in compensation, which might increase the frequency of the targeted gene disruption.

In conclusion, coinjection of exonucleases *Exo1* with TALENs provides an easy and efficient approach for gene knockouts in zygotes, and represents a promising breakthrough for gene targeting technologies applicable to various species.

Methods

Animals. All animal care and experiments conformed to the Guidelines for Animal Experiments of Kyoto University, and were approved by the Animal Research Committee of Kyoto University. Novel developed DA-*Tyr*^{em1Kyo} albino rats (NBRP-Rat No.0666) were deposited into the National Bio Resource Project – Rat in Japan (www.anim.med.kyoto-u.ac.jp/nbr).

Construction of TALEN plasmids and single-strand annealing (SSA) assay. The protocol for TALEN assembly was as previously reported[18,19]. Repeat assembly was conducted using a Golden Gate reaction, transformed into XL1-Blue competent cells and screened for precisely assembled clones by colony PCR using the pCR8_F1 and pCR8_R1 primers[19]. Constructed array plasmids and the appropriate last repeat were joined directly into the mammalian expression vectors, pcDNA-TAL or

A

Injected mRNA	Injected embryos	Two-cell embryos (%)	Pups (%)	♂	♀	Mutants (%)
TALEN	127	40 (31.5)	9 (23.0)	5	4	0 (0)
TALEN-NC	201	86 (42.8)	20 (23.3)	10	10	0 (0)
TALEN (Cellectis)	290	92 (31.7)	30 (32.6)	14	16	2 (6.7)
TALEN–NC + Exo1	68	29 (42.6)	12 (41.4)	7	5	3 (25.0)

B

C

gT-NC-Exo1-#1

TATAATAGCCATCAGGTT----------(Δ29bp)----------ATTACGTAATCCT

gT-NC-Exo1-#7

TATAATAGCCATCAGGTTTTATGTGATGGAACACCTGAGGGACCACTATTACGTAATCCT
TATAATAGCCATCAGG---------(Δ24bp)---------GACCACTATTACGTAATCCT

gT-NC-Exo1-#8

TATAATAGCCATCAGGTTTTATGTGATGGAACACCTGAGGGACCACTATTACGTAATCCT
TATAATAGCCATCAGGTTTTATGTGATG-----CCTGAGGGACCACTATTACGTAATCCT

Figure 3 | Efficient generation of knockout rats using TALENs with *Exo1*. (A) Microinjection of TALENs, TALENs-NC, TALENs from Cellectis, and TALENs-NC with *Exo1* into fertilized eggs of agouti DA rats. Coinjection of TALEN-NC mRNA with *Exo1* mRNA provided higher mutational efficiency (25%) in pups. (B) The white coat-color of an albino male rat (right) obtained by coinjection of TALEN-NC and *Exo1*. An agouti male (left) is a littermate. (C) Sequence analyses on founder rats showed a homozygous 29-bp deletion in *Tyr* (gT-NC-*Exo1*-#1). Microhomologous sequences adjacent to the breakpoint are underlined.

pcDNA-TAL-NC[18]. Final assembly, transformation and colony PCR screening for the second Golden Gate reaction were performed as previously reported[18,19].

The SSA assay was carried out as previously described[9]. The pGL4-SSA reporter vector was generated, containing inactive fragments of the luciferase gene, which bear 700-bp regions of homologous overlap and are driven by a cytomegalovirus (CMV) immediate-early enhancer/promoter. For the addition of TALEN target sequences, sense and antisense oligonucleotides, Sense: 5'- GTCGGATATAATAGCCATC-AGGTTTTATGTGATGGAACACCTGAGGGACCACTATTACGTAATCCTGG-AGGT-3', and Antisense: 5'- CGGTACCTCCAGGATTACGTAATAGTGGTCC-CTCAGGTGTTCCATCACATAAAACCTGATGGCTATTATATC-3', were annealed and inserted into *Bsa*I sites between the dissected luciferase elements of pGL4-SSA. For the ZFN positive control, a ZFN expression vector, pSTL-ZFA36, was constructed, as previously described[9].

Rat *Exo1* cDNA cloning. To clone the rat *Exo1* cDNA, first strand cDNA was isolated using the oligo(dT)12-18 primer and SuperscriptII reverse transcriptase (Life Technologies, Carlsbad, CA, USA) synthesized from total RNA extracted from the brain of F344 rats by the Isogen reagent (Nippon Gene, Tokyo, Japan). RT-PCR was performed with the primers: 5'-GGGCCATGCCTGTTTATTC-3' and 5'-TGTTACCAGTGTGTTACCAGTCG-3'. RT-PCR products were inserted into pGEM-T Easy (Promega, Fitchburg, USA) and sequenced to confirm the sequence. For expression *in vitro*, the full-length cDNA was subcloned into pcDNA6.2/V5/GW/D-TOPO (Life Technologies).

Cell culture and transfection. Rat fibroblast-like (Rat-1) cells were obtained from the RIKEN BRC Cell Bank (Tsukuba, Japan, http://www.brc.riken.jp/lab/cell/english). The Rat-1 cells were cultured in DMEM (Invitrogen), supplemented with 10% FBS (fetal bovine serum, CBB) in a humidified atmosphere containing 5% CO_2 at 37°C. The cells (1×10^5) were suspended in 10 μl R buffer (supplied as part of the Neon Transfection System, Invitrogen), given 0.5 μg of each plasmid, and electroporated under the following conditions: pulse voltage, 1300 V; pulse width, 20 ms; and pulse

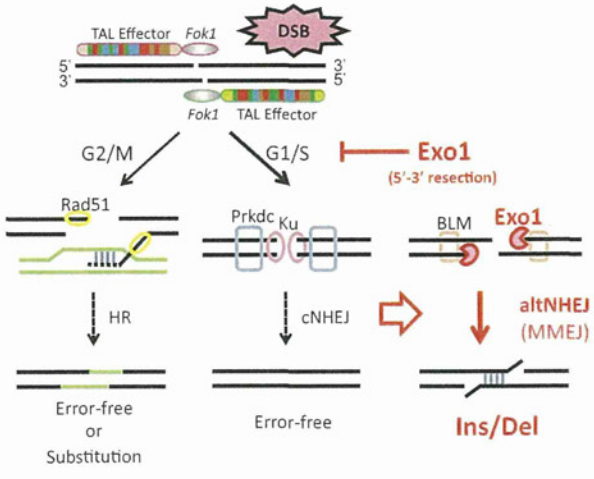

Figure 4 | Schematics of exonucleases (*Exo1*) functions in double-stranded break (DSB) repair pathways. Alternative NHEJ (altNHEJ), or microhomology mediated end-joining (MMEJ), generally repairs DSBs in the absence or failure of the classical NHEJ (cNHEJ) pathway[27–29]. Overexpression of *Exo1* induces increased recessions of DNA-ends at the DSB created by TALENs, which inhibits cNHEJ (See Supplementary Fig. S3) and enhances the mutagenic DSB-repair via altNHEJ, resulting in more indel mutations at the targeted gene.

number, 2 (program #15). Following electroporation, the cells were cultured in the medium described above without antibiotics for 24 h and then in the medium with antibiotics for 48 h. The *in vitro* transfer experiment was replicated three times.

Surveyor assay and DNA sequencing. For the Surveyor assay to detect TALEN-induced mutations, the SURVEYOR Mutation Detection Kit (Transgenomic, Omaha, NE, USA) was used in accordance with the manufacturer's protocol. Briefly, 72 h after electroporation, genomic DNA was extracted from the Rat-1 cells using Nucleospin (Macherey-Nagel, Düren, Germany). PCR was then performed using PrimeSTAR HS DNA polymerase (Takara Bio, Shiga, Japan), a high-fidelity enzyme, under the following conditions: 95°C for 1 min; followed by 95°C for 30 s, 68°C for 30 s, and 72°C for 1 min for 35 cycles. The PCR primers were as follows: 5′-TTGCATAAATTGGTTTTCACAGA-3′ and 5′-ATTTAAACATGAAAATAT-TACCTTCCA-3′. The PCR amplification products were heat denatured, digested by the Surveyor nuclease, and subjected to agarose gel electrophoresis to confirm TALEN-induced mutations.

For DNA sequencing analysis, the PCR products were subcloned into pCR4Blunt-TOPO plasmid vector (Life Technologies). Plasmids were extracted from the resultant *Escherichia coli* colonies for DNA sequencing. Sequencing was performed using the BigDye Terminator Cycle Sequencing Kit and an ABI PRISM 3130 Genetic Analyzer (Life Technologies).

Rat embryo culture. Pronuclear stage embryos were collected from DA/Slc females at 7 weeks of age that had undergone super-ovulation by injection with PMSG (Serotropin, Aska Pharmaceutical Co., Tokyo, Japan) and hCG (Gonatropin, Aska Pharmaceutical Co.). The GenomPlex Single Cell Whole Genome Amplification Kit (WGA4; Sigma Aldrich, St. Louis, MO, USA) was used to generate proprietary amplification of genomic DNA with universal oligonucleotide primers from a two-cell embryo. After purification, the single cell WGA products were analyzed the Surveyor assay and DNA sequencing analysis.

Microinjection of TALENs mRNA. To prepare mRNA of TALENs, TALEN-encoding expression plasmids were linearized with *Xho*I and extracted with phenol-chloroform by standard methods. To prepare the mRNA for *Exo1*, the *Exo1* plasmids were linearized with *Spe*I. Messenger RNA was transcribed *in vitro* using a MessageMax™ T7 mRNA transcription kit (Illumina, San Diego, CA, USA) and polyadenylated using a A-Plus™ Poly(A) polymerase tailing kit (Illumina). The resultant mRNA was purified using a MEGAClear™ kit (Illumina) and finally resuspended in RNase-free water at 10 ng/μl for each TALEN or *Exo1*. Approximately 2-3 pL of capped mRNA were injected into the male pronuclei of zygotes by microinjection[13]. The injected embryos were cultured in mKRB at 37°C with 5% CO_2 and 95% humidified air to promote their recovery. Surviving embryos were transferred to the oviducts of pseudopregnant Wistar females.

NHEJ and HR assays. NHEJ and HR assays were performed as previously reported[20,30,31]. MRC5SV-pEJ cells were used for the NHEJ assay. U2OS-DRGFP, HeLa-DRGFP and MRC5SV-DRGFP were used for the HR assay. To measure the repair of I-SceI-generated DSBs, 50 μg of the I-SceI expression vector (pCBASce) with or without a human *Exo1* expression plasmid (30 μg) was introduced into 5×10^6 cells by electroporation (GenePulser; Bio-Rad, Hercules, CA, USA). To determine the level of NHEJ or HR repair, the percentage of GFP-positive cells was quantified by flow cytometry (FACSCalibur; Becton Dickinson, Franklin Lakes, NJ, USA) 3 days after electroporation.

1. Carroll, D. Genome engineering with zinc-finger nucleases. *Genetics* **188**, 773–782 (2011).
2. Porteus, M. H. & Carroll, D. Gene targeting using zinc finger nucleases. *Nat Biotechnol* **23**, 967–973 (2005).
3. Rahman, S. H., Maeder, M. L., Joung, J. K. & Cathomen, T. Zinc-finger nucleases for somatic gene therapy: the next frontier. *Hum Gene Ther* **22**, 925–933 (2011).
4. Urnov, F. D., Rebar, E. J., Holmes, M. C., Zhang, H. S. & Gregory, P. D. Genome editing with engineered zinc finger nucleases. *Nat Rev Genet* **11**, 636–646 (2010).
5. Bogdanove, A. J. & Voytas, D. F. TAL effectors: customizable proteins for DNA targeting. *Science* **333**, 1843–1846 (2011).
6. DeFrancesco, L. Move over ZFNs. *Nat Biotechnol* **29**, 681–684 (2011).
7. Mussolino, C. & Cathomen, T. TALE nucleases: tailored genome engineering made easy. *Curr Opin Biotechnol* **23**, 644–650 (2012).
8. Scholze, H. & Boch, J. TAL effectors are remote controls for gene activation. *Curr Opin Microbiol* **14**, 47–53 (2011).
9. Ochiai, H. *et al.* Targeted mutagenesis in the sea urchin embryo using zinc-finger nucleases. *Genes Cells* **15**, 875–885 (2010).
10. Watanabe, T. *et al.* Non-transgenic genome modifications in a hemimetabolous insect using zinc-finger and TAL effector nucleases. *Nat Commun* **3**, 1017 (2012).
11. Ansai, S. *et al.* Targeted disruption of exogenous EGFP gene in medaka using zinc-finger nucleases. *Dev Growth Differ* **54**, 546–556 (2012).
12. Geurts, A. M. *et al.* Knockout rats via embryo microinjection of zinc-finger nucleases. *Science* **325**, 433 (2009).
13. Mashimo, T. *et al.* Generation of knockout rats with X-linked severe combined immunodeficiency (X-SCID) using zinc-finger nucleases. *PLoS One* **5**, e8870 (2010).
14. Cui, X. *et al.* Targeted integration in rat and mouse embryos with zinc-finger nucleases. *Nat Biotechnol* **29**, 64–67 (2011).
15. Miller, J. C. *et al.* A TALE nuclease architecture for efficient genome editing. *Nat Biotechnol* **29**, 143–148 (2011).
16. Certo, M. T. *et al.* Coupling endonucleases with DNA end-processing enzymes to drive gene disruption. *Nat Methods* **9**, 973–975 (2012).
17. Kuramoto, T. *et al.* Origins of albino and hooded rats: implications from molecular genetic analysis across modern laboratory rat strains. *PLoS One* **7**, e43059 (2012).
18. Sakuma, T. *et al.* Efficient TALEN construction and evaluation methods for human cell and animal applications. *Genes Cells* (in press).
19. Cermak, T. *et al.* Efficient design and assembly of custom TALEN and other TAL effector-based constructs for DNA targeting. *Nucleic Acids Res* **39**, e82 (2011).
20. Mashimo, T. *et al.* Generation and characterization of severe combined immunodeficiency rats. *Cell Rep* **2**, 685–694 (2012).
21. Mussolino, C. *et al.* A novel TALE nuclease scaffold enables high genome editing activity in combination with low toxicity. *Nucleic Acids Res* **39**, 9283–9293 (2011).
22. Bernstein, K. A. & Rothstein, R. At loose ends: resecting a double-strand break. *Cell* **137**, 807–810 (2009).
23. Huertas, P. DNA resection in eukaryotes: deciding how to fix the break. *Nat Struct Mol Biol* **17**, 11–16 (2010).
24. Longhese, M. P., Bonetti, D., Manfrini, N. & Clerici, M. Mechanisms and regulation of DNA end resection. *EMBO J* **29**, 2864–2874 (2010).
25. Mimitou, E. P. & Symington, L. S. DNA end resection--unraveling the tail. *DNA Repair (Amst)* **10**, 344–348 (2011).
26. Tran, P. T., Erdeniz, N., Symington, L. S. & Liskay, R. M. EXO1-A multi-tasking eukaryotic nuclease. *DNA Repair (Amst)* **3**, 1549–1559 (2004).
27. McVey, M. & Lee, S. E. MMEJ repair of double-strand breaks (director's cut): deleted sequences and alternative endings. *Trends Genet* **24**, 529–538 (2008).
28. Mladenov, E. & Iliakis, G. Induction and repair of DNA double strand breaks: the increasing spectrum of non-homologous end joining pathways. *Mutat Res* **711**, 61–72 (2011).
29. Symington, L. S. & Gautier, J. Double-strand break end resection and repair pathway choice. *Annu Rev Genet* **45**, 247–271 (2011).
30. Kobayashi, J., Kato, A., Ota, Y., Ohba, R. & Komatsu, K. Bisbenzamidine derivative, pentamidine represses DNA damage response through inhibition of histone H2A acetylation. *Mol Cancer* **9**, 34 (2010).
31. Pierce, A. J. & Jasin, M. Measuring recombination proficiency in mouse embryonic stem cells. *Methods Mol Biol* **291**, 373–384 (2005).

Author contributions

T.M. designed the work, produced all the data, and wrote the paper. T.K. and B.V. performed microinjection of TALENs into rat embryos. T. Sakuma and T.Y. constructed the TALENs. J.K. and Y.K. helped with *in vitro* experiments. T. Serikawa supervised the work. All authors read and corrected the manuscript before submission.

Additional information

Supplementary information accompanies this paper at http://www.nature.com/scientificreports

Competing financial interests: The authors declare no competing financial interests.

How to cite this article: Mashimo, T. *et al.* Efficient gene targeting by TAL effector nucleases coinjected with exonucleases in zygotes. *Sci. Rep.* **3**, 1253; DOI:10.1038/srep01253 (2013).

Cell Reports
Resource

Generation and Characterization of Severe Combined Immunodeficiency Rats

Tomoji Mashimo,[1,*] Akiko Takizawa,[1] Junya Kobayashi,[2] Yayoi Kunihiro,[1] Kazuto Yoshimi,[1] Saeko Ishida,[1] Koji Tanabe,[3] Ami Yanagi,[5] Asato Tachibana,[5] Jun Hirose,[4] Jun-ichiro Yomoda,[4] Shiho Morimoto,[1] Takashi Kuramoto,[1] Birger Voigt,[1] Takeshi Watanabe,[4] Hiroshi Hiai,[1] Chise Tateno,[5,6] Kenshi Komatsu,[2] and Tadao Serikawa[1]

[1]Institute of Laboratory Animals, Graduate School of Medicine
[2]Genome Repair Dynamics, Radiation Biology Center
[3]Department of Reprogramming Science, Center for iPS Cell Research and Application
[4]Center for Innovation in Immunoregulative Technology and Therapeutics, Graduate School of Medicine
Kyoto University, Kyoto 606-8501, Japan
[5]PhoenixBio. Co., Ltd., Higashihirosima, Hiroshima 739-0046, Japan
[6]Liver Research Project Center, Hiroshima University, Hiroshima 734-8551, Japan
*Correspondence: tmashimo@anim.med.kyoto-u.ac.jp
http://dx.doi.org/10.1016/j.celrep.2012.08.009

SUMMARY

Severe combined immunodeficiency (SCID) mice, the most widely used animal model of DNA-PKcs (*Prkdc*) deficiency, have contributed enormously to our understanding of immunodeficiency, lymphocyte development, and DNA-repair mechanisms, and they are ideal hosts for allogeneic and xenogeneic tissue transplantation. Here, we use zinc-finger nucleases to generate rats that lack either the *Prkdc* gene (SCID) or the *Prkdc* and *Il2rg* genes (referred to as F344-*scid gamma* [FSG] rats). SCID rats show several phenotypic differences from SCID mice, including growth retardation, premature senescence, and a more severe immunodeficiency without "leaky" phenotypes. Double-knockout FSG rats show an even more immunocompromised phenotype, such as the abolishment of natural killer cells. Finally, xenotransplantation of human induced pluripotent stem cells, ovarian cancer cells, and hepatocytes shows that SCID and FSG rats can act as hosts for xenogeneic tissue grafts and stem cell transplantation and may be useful for preclinical testing of new drugs.

INTRODUCTION

DNA-dependent protein kinase catalytic subunits (DNA-PKcs) are critical components of the nonhomologous end-joining (NHEJ) pathway of the DNA double-strand break (DSB) repair system. DSBs are usually generated by environmental influences such as ionizing radiation (IR) or by chemical mutagens, or are created during programmed processes such as V(D)J recombination or class switch recombination (CSR), which occur during lymphocyte development (Franco et al., 2006; Mahaney et al., 2009; Shrivastav et al., 2008; Yan et al., 2007). The Ku70/80 heterodimer first binds to the ends of the DSBs and recruits DNA-PKcs to form the active DNA-PK complex. Subsequently, together with Artimis, DNA-PKcs stimulate the processing of the DNA ends. Finally, the LIG4 complex, comprising LIG4, XRCC4, and XLF, seals the DSBs generated during NHEJ. Humans and several types of mammals with a defect in the genes involved in NHEJ cannot complete V(D)J recombination. This blocks lymphocyte development, resulting in severe combined immunodeficiency (SCID) (Bosma et al., 1983; O'Driscoll and Jeggo, 2006; Perryman, 2004; van der Burg et al., 2009). SCID mice, which arose spontaneously due to the defective DNA-PKcs gene (*Prkdc*), show an immunodeficient phenotype and increased sensitivity to IR (Bosma et al., 1983). In contrast, no *PRKDC* mutations had been reported in humans until recently, when a hypomorphic mutation with *PRKDC* kinase activity was identified in a patient with SCID with sensitivity to IR (RS-SCID; van der Burg et al., 2009). Although complete *PRKDC* deficiency is expected to be lethal in humans, spontaneous null mutations in the *PRKDC* gene were reported in Arabian horses and Jack Russell terriers, highlighting the fact that *PRKDC* deficiency is not tolerated equally in all species (Perryman, 2004).

SCID animals are widely used in biomedical research as hosts for allogeneic and xenogeneic tissue grafts. Humanized mice (i.e., immunodeficient mice engrafted with human cells or tissues, such as human hematopoietic stem cells [hHSCs], hepatocytes, or tumor cells) are powerful tools that have enabled scientists to gain greater insights into many human diseases (Azuma et al., 2007; Baiocchi et al., 2010; Brehm et al., 2010; Denton and García, 2011; Ito et al., 2008; Katoh et al., 2008; Kneteman and Mercer, 2005; Leonard, 2001; Meuleman et al., 2005; Pearson et al., 2008; Quintana et al., 2008; Shultz et al., 2007; Wege et al., 2008). Although the laboratory rat is an ideal model for physiological, pharmacological, toxicological, and transplantation studies, there are no reports of spontaneous, or gene-targeted, SCID rats. Recently, several strategies have been developed to produce a wide variety of genomic alterations in rats (Geurts et al., 2009; Izsvák et al., 2010; Mashimo et al., 2008; Tesson et al., 2011), including embryonic-stem-cell-derived p53 knockout rats (Tong et al., 2010). Other investigators

Cell PRESS
Open ACCESS

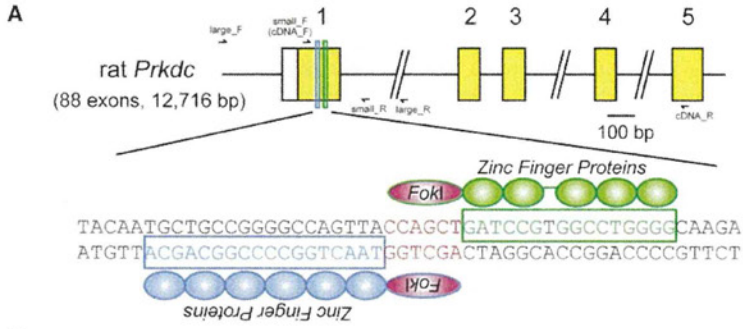

B

Strain	Targeted gene	Injected oocytes	Survived embryos	Transferred oocytes (%)	Born (%)	Mutants (%)
F344/Stm	*Prkdc*	148	115 (77.7)	107 (72.3)	♂6, ♀10 (12.1)	♂3, ♀1 (25.0)
Crlj:WI	*Prkdc*	215	163 (75.8)	133 (61.9)	♂16, ♀7 (17.3)	♂15, ♀7 (95.7)
F344/Stm	*Prkdc* & *Il2rg*	219	128 (58.4)	85 (38.8)	♂6, ♀8 (16.5)	♂1, ♀1* (14.8)

*Double injection of *Prkdc* and *Il2rg* ZFN-encoding mRNA provided one female carrying mutations in both *Prkdc* and *Il2rg* genes.

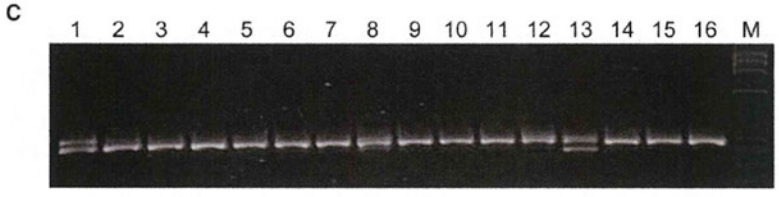

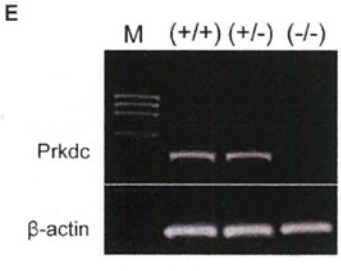

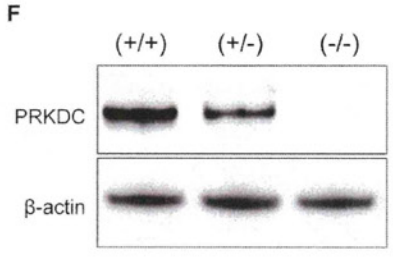

Figure 1. Injection of ZFN-Encoding mRNA into Rat Embryos Induces Targeted Loss-of-Function Mutations

(A) Schematic representation of the part of rat *Prkdc* gene. The magnified views illustrate the binding sites for the ZFN pairs.

(B) Injection of ZFN-encoding mRNA into F344/Stm or Crlj:WI rat fertilized oocytes.

(C) PCR analysis of 16 offspring obtained by ZFN injection of F344/Stm oocytes. M, DNA molecular weight marker φX174-HaeIII digest.

(D) Sequencing assay for ZFN-induced mutations in the target region in F344 rats. Multiple deletions and insertions are depicted by red dashes and letters, respectively, and are aligned along the WT sequences shown on the top line.

(E) RT-PCR analysis of *Prkdc* mRNA expression in the spleen of *Prkdc* (+/+, +/−, −/−) rats. *Gapdh* mRNA expression was used as an internal control.

(F) Western blot of PRKDC protein in the spleen of *Prkdc* (+/+, +/−, −/−) rats. β-actin was used as a loading control.

See also Figures S1 and S4.

and our group have also shown the successful application of zinc-finger nucleases (ZFNs) as a gene-targeting technology in rats, which is faster and more efficient than embryonic-stem-cell-mediated knockout technology (Cui et al., 2011; Geurts et al., 2009; Mashimo et al., 2010).

Here, we report the generation and characterization of single-knockout *Prkdc* (SCID) and double-knockout *Prkdc* and *Il2rg* (F344-*scid gamma* [FSG]) rats.

RESULTS

Generation of SCID Rats Using ZFNs

The design and validation of ZFN reagents targeting the first exon of rat *Prkdc* gene were described previously (Mashimo et al., 2010) (Figure 1A; Figure S1). The validated ZFN mRNA was microinjected into fertilized F344/Stm or Crlj:WI oocytes, which were then transferred into the oviducts of pseudopregnant Crlj:WI female rats (Figure 1B). Screening of 39 newborn animals revealed that 26 of them (66.7%) carried mutations, comprising deletions from 1 bp to 919 bp and a 1-bp insertion (Figures 1C and 1D; Figure S2). The rate and variation of the ZFN-induced mutations were similar to those reported in previous studies (Cui et al., 2011; Geurts et al., 2009; Mashimo et al., 2010). The majority of these were frame-shift mutations resulting in the complete loss of mRNA expression as confirmed by reverse transcriptase (RT)-PCR (Figure 1E) and protein expression as confirmed by western blotting (Figure 1F). Furthermore, double injection of *Prkdc* and

interleukin 2 receptor-gamma (*Il2rg*) ZFN-encoding mRNA into 219 fertilized F344/Stm oocytes resulted in one male carrying 7- and 46-bp deletions in *Prkdc,* and one female carrying 227- and 716-bp deletions in *Prkdc* and a 3-bp deletion in *Il2rg* (Figure 1B).

To clarify whether the ZFNs only induced mutations in the targeted region, we checked 12 sites that showed a high rate of similarity to the targeted site at the sequence level with no more than 7–8 bp mismatches, as illustrated in Table S1. Insertions or deletions were not observed at any of these off-target sites among the ZFN-modified founders. Although we cannot exclude the possibility that the ZFNs cleaved unknown off-target sites, we subsequently excluded such undesired mutations excluded from the genome of the carrier animals by backcrossing to the parental strain. After crossing with wild-type (WT) animals, the ZFN-induced *Prkdc* and *Il2rg* mutations were faithfully transmitted through the germline. Some of the ZFN-modified founders were subsequently bred to homozygosity for use in further experiments.

Growth Retardation in SCID Rats

Heterozygous $Prkdc^{+/-}$ rats were indistinguishable from their WT littermates in all respects. Approximately 25% of the offspring born to $Prkdc^{+/-}$ × $Prkdc^{+/-}$ crosses were homozygous $Prkdc^{-/-}$ rats, and were significantly smaller than their WT and heterozygous littermates (Figure 2A). When the embryos from $Prkdc^{+/-}$ × $Prkdc^{+/-}$ crosses were examined and weighed, a difference in size was observed at embryonic day 14.5 (E14.5), which became statistically significant at E17.5 (Figure 2B). During the 6 month observation period, the $Prkdc^{-/-}$ rats grew and maintained a body weight that was 70% of that of the controls (Figure 2C). $Prkdc^{-/-}$ SCID rats normally survive for at least 1 year under specific pathogen-free conditions. Both male and female $Prkdc^{-/-}$ rats were fertile, but the average litter size was small (4.7 ± 2.0 [n = 9] versus 9.1 ± 1.6 of F344 rats [n = 12]). Newly generated F344-$Prkdc^{-/-}$ $Il2rg^{-/-}$ rats (FSG rats) showed phenotypes similar to those of SCID rats for growth, survival, and reproducibility (Figure 2C).

To further characterize the growth deficiency, we derived primary fibroblasts from WT (+/+), heterozygous (+/−), and homozygous (−/−) rat embryos (rat embryonic fibroblasts [REFs]), and monitored their growth in vitro (Figure 2D). Early-passage $Prkdc^{-/-}$ REFs grew slowly, at a rate 70% of that shown by the $Prkdc^{+/-}$ and $Prkdc^{+/+}$ REFs. This difference was partly due to a decrease in the number of dividing cells within the $Prkdc^{-/-}$ cultures, as determined by incorporating bromodeoxyuridine (BrdU) into chromosomal DNA during an 18 hr labeling period (Figure 2E). Proliferation decreased with passage number, and by passage 4, $Prkdc^{-/-}$ REF cultures contained nondividing giant cells, suggesting premature senescence (Figure 2F). Senescence-associated β-galactosidase (SA-β-Gal) activity assays showed significantly higher numbers of SA-β-Gal-positive cells within $Prkdc^{-/-}$ REF cultures compared with $Prkdc^{+/-}$ or $Prkdc^{+/+}$ REF cultures (Figure 2G). To the best of our knowledge, neither growth retardation nor premature senescence has been reported in SCID mice (Bosma et al., 1983; Gao et al., 1998; Jhappan et al., 1997; Taccioli et al., 1998).

IR Sensitivity and DSB-Repair Defects in SCID REFs

Mouse embryonic fibroblasts (MEFs) from SCID mice or *Prkdc*-deficient mice, and the *Prkdc*-deficient human glioma cell line M059J are all IR-sensitive, although the level of sensitivity varies. When we used a colony survival assay to test IR sensitivity in REF cells, $Prkdc^{-/-}$ REFs were significantly more sensitive than $Prkdc^{+/-}$ or $Prkdc^{+/+}$ REFs (Figure 2H). Accordingly, $Prkdc^{-/-}$ REF cells accumulated foci comprising histone H2AX (γH2AX), a surrogate marker for DSBs, after an exposure to 1 Gy of irradiation (Figure 2I).

We next used a pEJ assay (Kobayashi et al., 2010) and a DR-GFP (Pierce and Jasin, 2005) assay to further examine the effects of *Prkdc*-deficiency on the NHEJ and homologous recombination (HR) pathways, respectively. After the generation of DSBs using I-SecI, the number of GFP-positive $Prkdc^{-/-}$ REFs in the pEJ assay significantly decreased compared with that of $Prkdc^{+/+}$ REFs (Figure 2J), clearly indicating a severe deficiency in the NHEJ pathway in these cells. In contrast, the HR pathway was significantly increased in $Prkdc^{-/-}$ REFs (Figure 2K), suggesting that a deficiency in the NHEJ pathway induces a more active HR pathway as a compensatory mechanism.

Impaired Lymphoid Development in SCID Rats

Gross and microscopic analyses of SCID and FSG rats revealed abnormal lymphoid development (Figures 3A–3D). The thymuses from SCID and FSG rats were extremely hypoplastic (Figure 3A) and comprised an epithelial rudiment without any lymphocytes (Figure 3C). The spleens were also smaller (Figure 3B), with severely hypoplastic white pulp, and red pulp containing myeloid cells (Figure 3D). Serum immunoglobulin (Ig) levels (IgA and IgM) were undetectable in 5-week-old $Prkdc^{-/-}$ rats, whereas IgG levels in $Prkdc^{-/-}$ rats nursed by $Prkdc^{+/-}$ heterozygous mothers were detected at half the levels seen in control $Prkdc^{+/+}$ rats (Figures 3E–3G), confirming the postnatal transfer of maternal IgG previously described in rodents (Gustafsson et al., 1994). IgG levels were lowest in 8-week-old $Prkdc^{-/-}$ rats, and undetectable in 5-week-old $Prkdc^{-/-}$ rats nursed by $Prkdc^{-/-}$ homozygous mothers (Figure 3E). Approximately 20% of young adult (or of the majority of old SCID) mice known to have a "leaky" phenotype showed detectable Ig levels, generated by a few clones of functional B cells (Bosma et al., 1983). To date, none of the SCID rats examined (n = 9, until 1 year of age) have shown a leaky phenotype for serum Ig (Figures 3E–3G).

Consistent with the histology, the number of thymocytes and splenocytes was markedly reduced in SCID and FSG rats compared with control F344 rats (Table S2). In the peripheral blood (PB) profile, the number of white blood cells (WBCs) was reduced in SCID and FSG rats compared with F344 rats (Table S3). Differential counts of WBCs showed a dramatic decrease in leucocytes and relative increases in neutrophils and monocytes in SCID and FSG rats (Table S4).

To further characterize the immunological deficiency in SCID rats, we examined cell populations isolated from the thymus, spleen, and bone marrow (BM) using flow cytometry (Figures 3H–3J). $CD4^+$ or $CD8^+$ single-positive (SP), and $CD4^+CD8^+$ double-positive (DP) T cells were completely absent from SCID

Cell PRESS
Open ACCESS

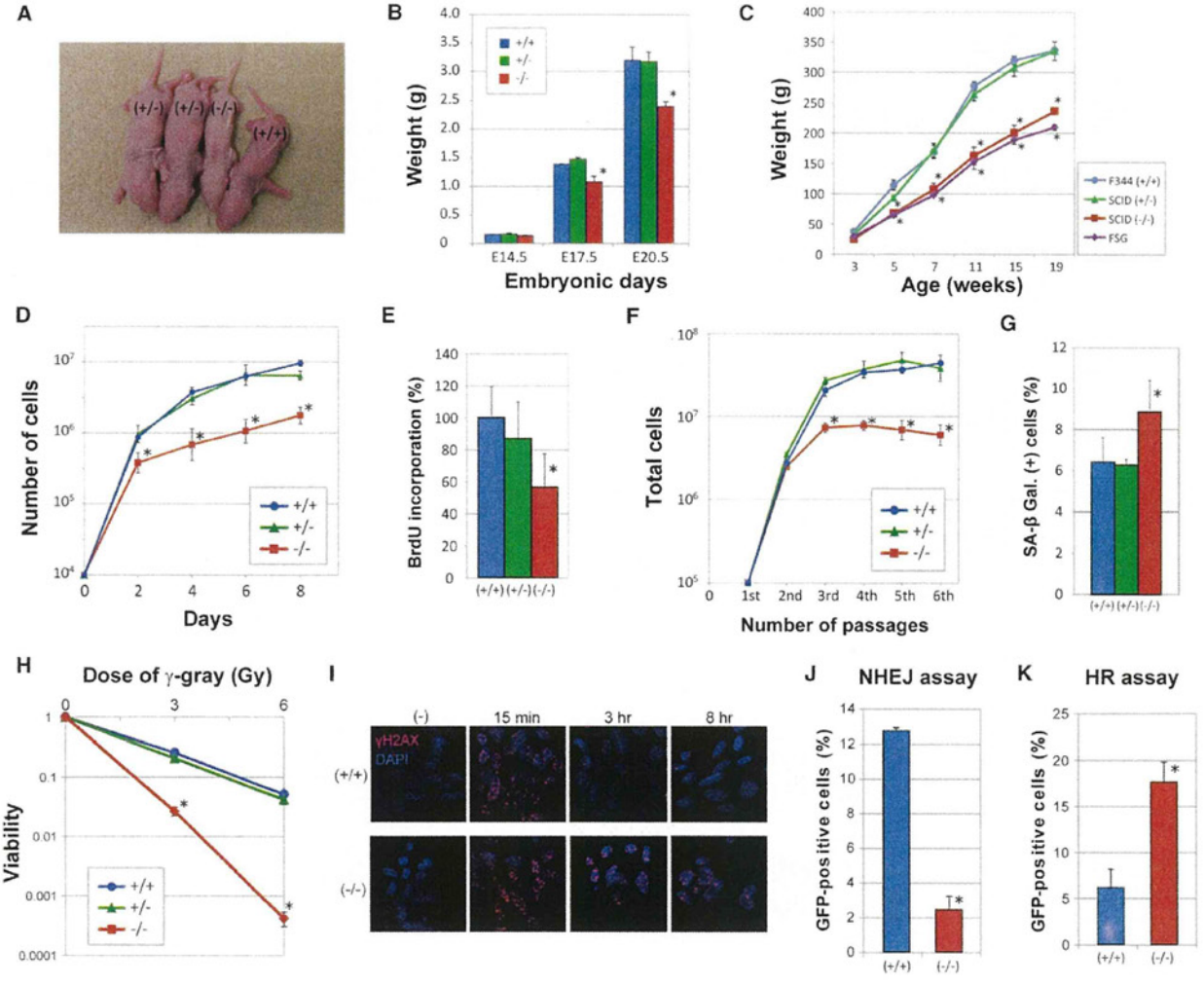

Figure 2. *Prkdc* Deficiency in Rats Results in Growth Retardation, Premature Senescence, and Radiation Sensitivity

(A) Photograph of newborn for *Prkdc*$^{-/-}$, *Prkdc*$^{+/-}$, and WT *Prkdc*$^{+/+}$ littermates.

(B) Development of *Prkdc* (+/+, n = 3; +/−, n = 6; −/−, n = 3) embryos, as measured by weight at E14.5, E17.5, and E20.5.

(C) Postnatal growth of *Prkdc* (+/+, n = 4; +/−, n = 8; −/−, n = 4) and *Prkdc*$^{-/-}$ *Il2rg*$^{-/y}$ FSG (n = 5) rats.

(D) Proliferation of primary fibroblasts from *Prkdc* (+/+, n = 3; +/−, n = 3; −/−, n = 3) E14.5 rats. Second-passage REFs were plated in 60 mm dishes and counted every 2 days.

(E) Division of REFs from *Prkdc* (+/+, n = 3; +/−, n = 3; −/−, n = 3) rats. Incorporation of BrdU into chromosomal DNA was measured after an 18 hr labeling period.

(F) Proliferation of REFs from *Prkdc* (+/+, n = 3; +/−, n = 3; −/−, n = 3) rats at each passage.

(G) Cell staining for senescence-associated SA-β-galactosidase activity. The percentage of SA-β-galactosidase-positive cells in the REF (+/+, n = 3; +/−, n = 3; −/−, n = 3) cells was calculated from the average from three experiments.

(H) Radiation sensitivity of *Prkdc* (+/+, +/−, −/−) REF cell lines. Cells were irradiated with the indicated dose of γ-rays, and viability was analyzed using colony formation assays.

(I) γ-H2AX focus formation assay in *Prkdc* (+/+, −/−) REF cell lines after exposure to 1 Gy of γ-rays. Cells were stained with anti-γ-H2AX antibody as a marker for DSBs.

(J and K) NHEJ activity and HR activity of *Prkdc* (+/+, −/−) REF cell lines. I-SceI expression plasmids were introduced into each REF cell line by electroporation. After 2 days, GFP-positive cells induced through the NHEJ pathway (J) or the HR pathway (K) were analyzed by flow cytometry.

Error bars indicate the mean ± SEM; *$p < 0.05$ for each genotype by one-way analysis of variance (C–H) or Student's t test (J and K). See also Figure S2.

thymuses but were abundant in control thymuses (Figure 3H). This was clearly different from SCID mice, in which DP T cells are present in the thymus (Gao et al., 1998; Taccioli et al., 1998). CD3$^-$CD45RA$^+$ B cells were completely absent from SCID spleens and BM, whereas CD3$^-$CD161a$^+$ natural killer (NK) cells were present or even increased (Figures 3I and 3J). NK cell numbers were mostly depleted in the BM and spleens of 5-week-old FSG rats (Figures 3I and 3J).

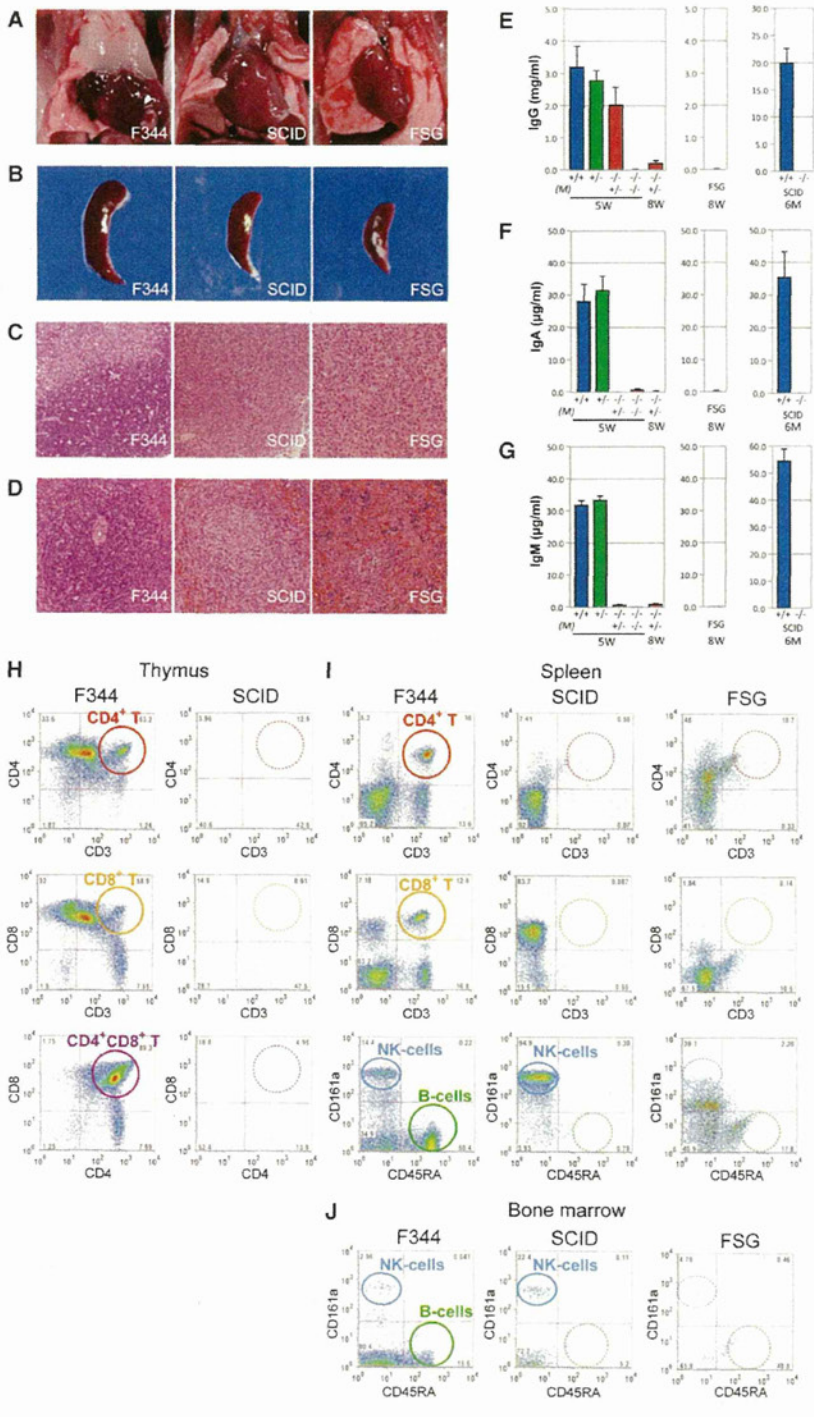

Figure 3. Abnormal Lymphoid Development in *Prkdc*-Deficient SCID Rats

(A and B) Pictures of thymus (A) and spleen (B) from F344, SCID, and FSG rats.

(C) Histological analysis of the thymus (×40). The thymuses of SCID and FSG rats were severely hypoplastic and consisted of an epithelial cell sheet.

(D) Histological analysis of the spleen (×100). In the spleens of SCID and FSG rats, the white pulp was virtually devoid of lymphocytes and the red pulp was occupied by a variety of myeloid cells.

(E–G) ELISA for serum IgG (E), IgA (F), and IgM (G) levels in *Prkdc* SCID (+/+, n = 3; +/−, n = 6; −/−, n = 4) rats. Error bars indicate the mean ± SEM. IgG, IgA, and IgM levels were very low or undetectable in 5-week-old $Prkdc^{-/-}$ rats nursed by $Prkdc^{-/-}$ homozygous mothers (M: −/−, n = 3), whereas IgG was detected in 5-week-old $Prkdc^{-/-}$ rats nursed by a $Prkdc^{+/-}$ heterozygous mother (M: +/−, n = 4) at half the levels seen in the control rats, probably due to transfer through the maternal milk. IgG, IgA, and IgM levels were undetectable in 8-week-old FSG rats (n = 4) and 6-month-old $Prkdc^{-/-}$ rats (+/+, n = 6; −/−, n = 5).

(H–J) Flow cytometric analysis of cell populations isolated from thymus (H), spleen (I), and BM (J) in SCID and FSG rats. Dot plots represent CD3, CD4, and CD8 cells for demarcation of T cell subpopulations, and CD3, CD45RA, and CD161a cells for differentiation of T cell, B cell, and NK cell subpopulations. $CD4^+$ and $CD8^+$ SP, and $CD4^-CD8^+$ DP T cells were absent from SCID thymuses (H). CD3 $CD45RA^+$ B cells were absent from the spleens (I) and BM (J) of SCID and FSG rats. $CD3^-CD161a^+$ NK cells were present in the SCID, but were mostly diminished in FSG rats (I and J).

Xenotransplantation of Human Induced Pluripotent Stem Cells and Tumor Cells

SCID mice can accept transplanted tissues from other species, including humans. We used SCID rats in a teratoma formation assay. Teratomas were induced by inoculation of human induced pluripotent stem (iPS) cells beneath the testis capsule (Takahashi et al., 2007). All SCID (n = 4/4) and FSG (n = 3/3) rats developed tumors, and in most cases, both testes were affected (Figure 4A). Histological examination showed that the lesion had displaced the normal testis and contained solid areas of teratoma. All teratomas contained differentiated tissues representing all three germ layers, including columnar epithelium, pseudostratified ciliated epithelium (endoderm), neural rosettes (ectoderm), cartilage, and adipose tissue (mesoderm; Figures 4B–4F).

To further evaluate the immunological defects, we used SCID and FSG rats as hosts for the xenotransplantation of human ovarian cancer cells (Mashimo et al., 2010). All SCID rats (n = 6/6) developed tumors within 14 days after injection of ovarian cancer cells, whereas control F344 rats showed no evidence of tumor growth

Cell PRESS
Open ACCESS

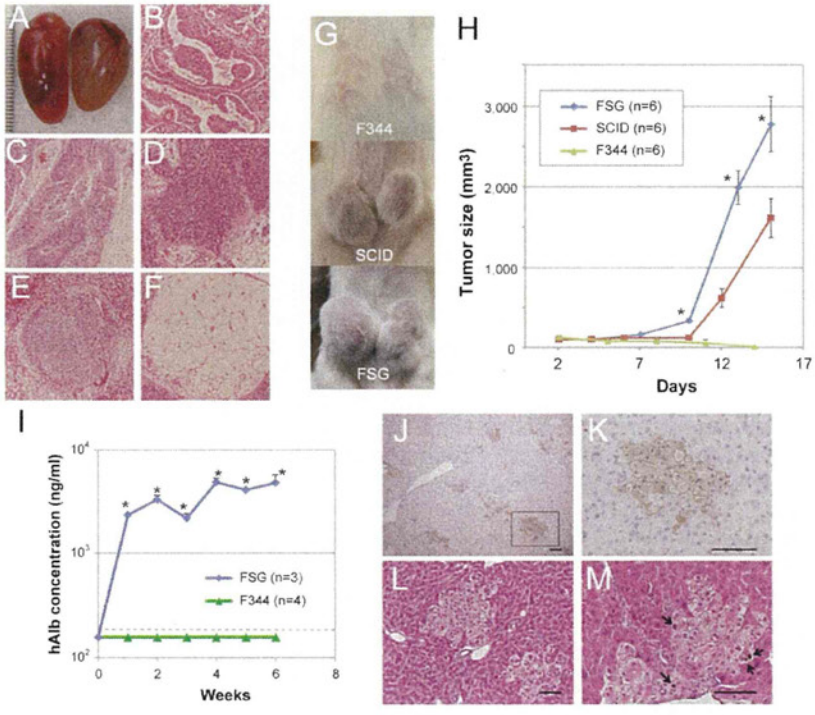

Figure 4. Xenotransplantation of Human iPS Cells, Tumor Cells, and Hepatocytes into SCID and FSG Rats

(A) Teratoma formation assay for human 201B7 iPS cells in the testis of SCID and FSG rats.

(B–F) Histology of differentiated elements found in teratomas: (B) columnar epithelium (endoderm), (C) pseudostratified ciliated epithelium, (D) neural rosettes (ectoderm), (E) cartilage (mesoderm), and (F) adipose tissue.

(G) Subcutaneous injection of human A2780 ovarian cancer cells into F344 (n = 6), SCID (n = 6), and FSG (n = 6) rats.

(H) Growth curve of human ovarian cancer cells. SCID rats developed tumors within 14 days after injection, whereas FSG rats showed more rapid cell proliferation, probably due to the lack of NK cells.

(I–M) Human hepatocytes were transplanted into retrorsine-treated infant FSG (n = 4) and control F344 (n = 3) rats. hAlb was detected in the blood of all transplanted FSG rats (I). The detection limit for hAlb (156.3 ng/ml) is indicated by the dotted line. Error bars indicate the mean ± SEM (H and J). *$p < 0.05$ for SCID versus FSG (H) and for F344 versus FSG (I) by Student's t test.

(J and K) Liver sections stained with human cytokeratin 8/18 (hCK8/18) show engraftment and repopulation of donor human hepatocytes in the recipient rat livers. The sections were counterstained with hematoxylin. The region enclosed by the square in (J) is magnified in (K).

(L) Colonies of cells with a clear cytoplasm were observed in liver sections stained with H&E. The cells were uniform in size, and most were mononuclear.

(M) Proliferated human hepatocytes were labeled with BrdU as shown by arrows. The sections were counterstained with H&E.

Bars = 100 μm (J–M). See also Figure S3.

(n = 0/6; Figure 4G). Of interest, human cancer cells proliferated more rapidly in FSG rats (n = 6/6), presumably due to the lack of NK cell activity in these animals (Figure 4H). The tumors were confirmed by histological analysis, and by PCR using primers to amplify the human MHC class II DQB2 region. These observations illustrate the impaired immune system of SCID and FSG rats, and clearly show that these animals will be useful models for cancer and stem cell research.

Transplantation of Human Hepatocytes and hHSCs

The different metabolic enzyme profiles in human and rat livers are a major limitation for toxicology and drug testing. We generated liver-humanized rats by injecting human hepatocytes into the livers of infant FSG rats pretreated with a pyrrolizidine alkaloid (retrorsine) that is toxic to hepatocytes (Figures 4I–4M). In this study we used FSG rats because they have more immunocompromised states compared with SCID rats, as observed in the tumor cell engraftment. Human albumin (hAlb) was detectable in the blood of all FSG rats ($>1 \times 10^3$ ng/ml, n = 3) 1 week after transplantation (Figure 4I). The hAlb levels increased until 6 weeks after transplantation. However, hAlb was not detectable in F344 control rats (n = 4). Small clusters of human cytokeratin 8/18 (hCK8/18)-positive cells were observed in the livers of the transplanted FSG rats, indicating the successful engraftment and repopulation of human hepatocytes at the tissue level (Figures 4J and 4K). The human hepatocytes within these colonies were morphologically normal but their cytoplasm appeared to be clear (Figure 4L), probably because of the high glycogen content previously reported in liver-humanized mice (Tateno et al., 2004). The BrdU-positive donor cells within the colonies represented the proliferation of engrafted human hepatocytes in the livers of FSG rats (Figure 4M).

The engraftment of hHSCs in immunodeficient mice, such as SCID-hu models (Brehm et al., 2010; Denton and García, 2011; McCune et al., 1989; Pearson et al., 2008; Shultz et al., 2007; Wege et al., 2008), provides an opportunity to study the human immune system in vivo. To test the capability of this feature, we injected human cord blood (hCB) $CD34^+$ cells into 4-week-old FSG rats. During the 3-month monitoring period after transplantation, no human $CD45^+$ cells could be detected in the PB of hHSC-transplanted FSG rats (Figure S3A). Neither human CD3+ T cells nor CD19+ B cells were detected in the PB, spleen, or BM (Figure S3B). Furthermore, 6 months after transplantation, no human $CD45^+$ cells were detected in FSG rats (Figure S3C).

DISCUSSION

In this study, we successfully generated *Prkdc*-deficient SCID rats by using the ZFN technology. The SCID rats were significantly different from SCID mice, in that they showed growth retardation, defects in fibroblast proliferation, and a more severe immunodeficient phenotype. This suggests that DNA-PKcs have

distinct functions in mice and rats. Although few studies have examined spontaneous null mutations in human DNA-PKcs, it has been reported that gene-targeting disruption of human somatic cells results in profound growth retardation, IR sensitivity, and increased genetic instability (Ruis et al., 2008). The most reasonable explanation for the phenotypic differences between mice and humans is that human cells express 50 times more DNA-PK activity than rodent cells (Finnie et al., 1995). Our expression analysis of spleen and fibroblast cells showed that humans express many more DNA-PKcs compared with rodents, and rats express three times more compared with mice (Figure S2). Although DNA-PKcs play a major role in DSB repair (as do other members of the phosphatidylinositol 3-kinase-related kinase [PIKK] family, including ATM and ATR), their exact role is still not completely understood. There are at least three DSB repair pathways: NHEJ, HR, and the alternative NHEJ pathway (Mahaney et al., 2009; Shrivastav et al., 2008; Zha et al., 2011). The pathway used for DSB repair seems to differ between species. NHEJ, in which DNA-PKcs play a key role, is considered to be an error-prone pathway, whereas HR (the major process in lower eukaryotes that lack a DNA-PKcs enzyme) is error-free. Considering that much of the genome in higher eukaryotes comprises less-well-conserved noncoding DNA, NHEJ may have evolved along with DNA-PK activity, particularly in higher mammalian species.

Although SCID mice are the most commonly used experimental animal model for xenograft transplantation, the normal NK cell activity observed in these animals contributes to the limited longevity and function of transplanted human cells (Shultz et al., 2007). Therefore, we additionally generated FSG rats, which show no such NK cell activity. Although both SCID and FSG rats could serve as hosts for xenogeneic cell grafts such as human iPS cells and ovarian cancer cells, the FSG rats showed higher proliferation of human tumor cells than the SCID rats (Figure 4H), indicating a more severely immunocompromised state similar to that reported in *Prkdc*- and *Il2rg*-deficient mice used for xenotransplantation of human melanoma cells (Quintana et al., 2008) or human blood cells (Ishikawa et al., 2005). Further transplantation studies using diverse human cancer cells, such as preclinical cancer cells or cancer stem cells, will be interesting and will improve our understanding of severely immunocompromised hosts.

In addition, we engrafted human hepatocytes into the livers of retrorsine-treated FSG rats (Figure 4I–4M). hAlb was secreted in the blood of transplanted FSG rats, and clusters of human transplanted hepatocytes were observed in the livers of the FSG rats. Liver-humanized rats have several advantages over mouse models: (1) rats are 10 times larger than mice, providing greater blood volumes and more bile acid, cells, and tissues; (2) pharmacological and toxicological data have been accumulated for rats; and (3) it is easier to perform complex surgical experiments in rats. Liver-humanized rats may also allow large-scale and high-quality proliferation of either WT human hepatocytes or iPS-derived hepatocytes, which is currently a considerable obstacle to the culture of human hepatocytes. Liver-humanized rats would provide a robust platform for in vivo toxicological assays and drug metabolism assays. Although the replacement rate of human hepatocytes in the FSG rats was still lower compared than that previously obtained in liver-humanized mice (Azuma et al., 2007; Strom et al., 2010; Tateno et al., 2004) that were genetically modified using either uroplasminogen activator (*uPA*) transgenes (Tateno et al., 2004) or Fumaryl acetoacetate hydrolase (*Fah*) knockouts (Strom et al., 2010), similar genetic alterations in rats will probably also improve the engraftment success in liver-humanized rats.

Despite these successful results for transplantation of human iPS cells, tumor cells, and hepatocytes, the FSG rats rejected transplanted hHSCs (Figure S3). In mice, xenotransplantation in the nonobese diabetic *Prkdc*^{scid} (NOD.SCID) or NOD.*Prkdc*^{scid}.*Il2rg*$^{-/-}$ (NSG or NOG) mouse has become the gold-standard assay for hHSCs, highlighting the importance of the genetic background for such transplantation experiments. Recently, it was shown that the signal regulatory protein alpha (*Sirpa*) of the NOD allele enhances binding to the human CD47 and could provide inhibitory regulation of mouse phagocytes by CD47-SIRPa interaction (the so-called "don't eat me" signal), allowing significantly increased engraftment and maintenance of hHSCs in the mouse BM (Takenaka et al., 2007). This was also supported by experiments in which transgenic mice with human SIRPa in the non-NOD background showed significantly higher levels of human cell engraftment comparable to those in NSG mice (Strowig et al., 2011). Transgenic FSG rats with human SIRPa or NOD-SIRPa may change the BM microenvironment of FSG rats in a way that allows them to accept the engraftment of hHSCs. In addition to *Sirpa*, structural species-specific differences in the BM environment between mice and rats, and differences in the protocols used for HSC engraftment may explain why transplantation of hHSCs fails in FSG rats.

In conclusion, the newly developed SCID and FSG rats described in this study can be a valuable resource in various fields, such as stem cell research and translational research, and serve as an important experimental model for preclinical drug testing. These humanized models will also allow preclinical evaluation of stem-cell-based therapies and expand the options for translational research. This is particularly important in the field of regenerative medicine, because humanized rats can be used to evaluate not only the ability of the cells to engraft but also their therapeutic efficiency. However, additional genetic modifications may be required to permit transplantation of human cells or tissues, such as human hepatocytes and hHSCs.

EXPERIMENTAL PROCEDURES

Generation of Knockout Rats Using ZFNs

Custom-designed ZFN plasmids for the rat *Prkdc* gene and the *Il2rg* gene were obtained from Sigma-Aldrich (St. Louis, MO). The design, cloning, and validation of the ZFNs were performed as previously described (Mashimo et al., 2010). In brief, ZFNs were designed to recognize a site-specific sequence within the first exon of the rat *Prkdc* gene (Figure S4). Approximately 2–3 pl of ZFN mRNA (10 ng/μl) were injected into the pronuclei of embryos collected from F344/Stm or Crlj:WI females as previously described (Mashimo et al., 2010). The cultured embryos were then transferred to the oviducts of pseudo-pregnant females (Crlj:WI, 8–10 weeks). To edit the ZFN cleavage site in the genome at the *Prkdc* locus, two primer sets were designed to amplify small (309 bp) and large (1,321 bp) fragments as shown in Figure S4. The PCR products were directly sequenced using the BigDye terminator v3.1 cycle sequencing mix and the standard protocol for an Applied Biosystems 3130 DNA Sequencer (Carlsbad, CA).

All animal care and experiments conformed to the Guidelines for Animal Experiments of Kyoto University, and were approved by the Animal Research Committee of Kyoto University. Transplantation studies using human hepatocytes were approved by the Ethics Board of PhoenixBio Co., Ltd. (Higashihiroshima, Japan). All SCID rats were maintained under specific pathogen-free conditions. The SCID rats are deposited in the National BioResource Project–Rat in Japan (http://www.anim.med.kyoto-u.ac.jp/nbr).

RT-PCR and Western Blotting

Total RNA was extracted from the spleens of 5-week-old rats using Isogen reagent (Nippon Gene, Tokyo, Japan). RT-PCR was performed using the primers for *Prkdc* described in Figure S2, and with *Gapdh* 5′-GGCACAGT CAAGGCTGAGAATG-3′ and 5′-ATGGTGGTGAAGACGCCAGTA-3′. Western blotting was carried out using cell lysates from the spleens of 5-week-old rats according to standard methods. Signals were detected with antibodies against rat PRKDC (H-163; Santa Cruz Biotechnology, Santa Cruz, CA) and β-actin (AC-40; Sigma Aldrich).

REF Culture, Proliferation Assays, and SA-β-Galactosidase Assay

REFs were isolated from embryos after 14.5 days of gestation from the female partners of intercrossed *Prkdc*$^{+/-}$ rats. To obtain a growth curve, passage 2 REFs (2×10^4) were plated on six-well plates in triplicate. The cells were trypsinized, stained with trypan blue, and counted every other day for a total of 8 days. For the BrdU incorporation assay, cells were plated with BrdU (100 μM) and labeled for 48 hr in 96-well plates. The cells were stained with the anti-BrdU-POD antibody and quantified by measuring the absorbance with an enzyme-linked immunosorbent assay (ELISA) reader (BrdU Labeling and Detection Kit III; Roche Applied Science, Indianapolis, IN). To assess SA-β-galactosidase activity, cells were plated 60 mm dishes and stained for 24 hr. The percentage of SA-β-galactosidase-positive cells was determined by manually counting the number of blue cells (Senescence Detection Kit; BioVision, Mountain View, CA) within the total cell population.

Preparation of Immortalized REF Cells

Generation of immortalized REF cells by human telomerase reverse transcriptase (hTERT) was performed as previously described (Nakamura et al., 2002). Briefly, rat primary fibroblasts (+/+, +/−, or −/−) were infected with an hTERT-introduced retrovirus and then continuously cultured with G418. After a few weeks, viable cells were infected with SV40 and then continuously cultured for >1 month. These transformed cells (REF-hTERT/SV) were used for radiation sensitivity assays, and HR and NHEJ assays.

Radiation Sensitivity Assay and Immunofluorescence Staining for γ-H2AX Foci

For the radiation sensitivity assays, the cells were trypsinized and irradiated with 3 or 5 Gy of ^{60}Co γ-rays at a dose rate of 1.1 Gy/min. Immediately after irradiation, the cells were plated into 100 mm dishes at a density such that 50–200 cells would survive, and then incubated for 10 days. The dishes were then fixed with ethanol and stained with 3% Giemsa, and the number of colonies was counted. The surviving fractions were calculated by comparing the number of colonies formed by irradiated cells with the number of colonies formed by nonirradiated control cells. Each result represents an average value from three independent experiments.

Immunostaining for γ-H2AX foci was performed as previously described (Kobayashi et al., 2010). Cells grown on a glass slide were fixed with cold methanol for 15 min, rinsed with cold acetone several times, and then air-dried. Anti-γ-H2AX antibody (Upstate: #05-636) and Alexa-596-conjugated anti-mouse IgG antibodies (Molecular Probes, Carlsbad, CA) were to visualize the γ-H2AX foci.

NHEJ and HR Assays

NHEJ and HR assays were performed as previously described (Kobayashi et al., 2010; Pierce and Jasin, 2005). The cells were generated from REF-hTERT/SV cells via introduction of a pEJ construct for the NHEJ assay or a DR-GFP construct for the HR assay. To measure the repair of I-SceI-generated DSBs, 50 μg of the I-SceI expression vector (pCBASce) was introduced into 1×10^6 cells by electroporation (GenePulser; Bio-Rad, Hercules, CA). To determine the level of NHEJ or HR repair, the percentage of GFP-positive cells was quantified by flow cytometry (FACSCalibur; Becton Dickinson, Franklin Lakes, NJ) 3 days after electroporation.

Immunofluorescence and Fluorescence-Activated Cell-Sorting Analysis

PB specimens were collected from the caudal vena cava. Serum Ig levels were measured by ELISA using Rat IgG, IgA, and IgM ELISA quantitation kits (Bethyl Laboratories, Montgomery, TX). For histopathology, tissues were fixed in Bouin's fluid and embedded in paraffin. The embedded tissues were then sectioned (5–7 μm thick) at room temperature and stained with hematoxylin and eosin (H&E) to permit evaluation by light microscopy.

Flow cytometric analysis of cell populations isolated from thymus, BM, and spleen were carried out using IOTest Anti-Rat CD3-FITC/CD45RA-PC7/CD161a-APC (Beckman Coulter, Fullerton, CA) to differentiate the T cell, B cell, and NK cell subpopulations, and IOTest Anti-Rat CD3-FITC/CD4-PC7/CD8-APC (Beckman Coulter) to enumerate the T cell subpopulations. Anti-CD45 monoclonal antibodies (Beckman Coulter) were used for the intracellular staining of lymphocytes. Mouse IgM, IgG1, and IgG2a antibodies (Beckman Coulter) were used as isotype-matched controls. The cell samples were treated with FcR-blocking reagent (Miltenyi Biotec, Auburn, CA) for 10 min, stained with the fluorochrome-conjugated antibodies for 30 min, and washed three times with PBS/10% FCS. Stained cell samples were analyzed with the use of a four-color fluorescence-activated cell-sorting (FACS) flow cytometer (FACSCalibur; Becton Dickinson) and the data were analyzed with CellQuest software (Becton Dickinson).

Teratoma Formation by Human iPS Cells

Human iPS cells (201B7) were supplied by the Center for iPS Cell Research and Application, Kyoto University (Kyoto, Japan). Clumps of ~2×10^5 human iPS cells with an undifferentiated morphology were harvested at the time of routine passage as described previously (Takahashi et al., 2007), and injected into the testis of 6- to 8-week-old rats. Six to 8 weeks later, when testicular lesions developed and were palpable, the resulting tumors were dissected, fixed in 10% neutral buffered formalin, embedded in paraffin, and examined histologically after H&E staining.

Tumor Cell Xenotransplantation

The human ovarian cancer cell line A2780 was purchased from the European Collection of Cell Cultures (ECACC, Wiltshire, UK). Cells were cultured in RPMI 1640 medium (GIBCO, Fort Worth, TX) with 10% heat-inactivated FBS (Hyclone, Logan, UT). Subcutaneous injections of 2×10^5 A2780 cells plus Matrigel (Becton Dickinson) were performed on 5-week-old female rats. Tumors were measured (length [*a*] and width [*b*]) in millimeters using calipers, and tumor volumes (*V*) were calculated using the formula $V = ab^2/2$, where *a* is the longer of the two measurements. Human-specific PCR primers were designed to amplify major histocompatibility complex class II DQ beta 2 (HLA-DQB2) at exon 4 as follows: 5′-CCTAGGGTGGTCAGACTGGA-3′ and 5′-AAAATCCCCCAAAACAAAGG-3′.

Transplantation of Human Hepatocytes

Human hepatocytes were isolated from human-hepatocyte chimeric mice (PXB mice, http://www.phoenixbio.co.jp) using the two-step collagenase perfusion method as described previously (Yamasaki et al., 2010). The donor cells (cryopreserved human hepatocytes derived from a 5-year-old boy) were purchased from BD Gentest (Becton Dickinson). Two-week-old rats were given intraperitoneal injections of retrorsine (Sigma-Aldrich) at 10 mg/kg body weight. Seven days after retrorsine treatment, the isolated human hepatocytes (5 or 10×10^5 viable cells) were transplanted into the animals via the portal vein. To deplete Kupffer cells, the rats were injected intraperitoneally with 10 ml/kg of liposome-encapsulated clodronate 2 days before and 3 days after transplantation. Plasma samples were collected weekly and hAlb levels were measured by ELISA (Human Serum Albumin ELISA Quantitation Kit; Bethyl Laboratories). The rat livers were harvested 6 weeks after transplantation. When necessary, BrdU (50 mg/kg; Sigma-Aldrich) was injected intraperitoneally 1 hr before sacrifice. Paraffin and frozen sections (5 μm thick) were prepared from the liver tissues and subjected to H&E or